Monthly Notices
of the
ROYAL ASTRONOMICAL SOCIETY

MNRAS **493,** 4748–4762 (2020)
Advance Access publication 2020 February 7

doi:10.1093/mnras/staa362

Impact of convective boundary mixing on the TP-AGB

G. Wagstaff,[1,2] M. M. Miller Bertolami[3,4]★ and A. Weiss[1]

[1]*Max-Planck-Institut für Astrophysik, Karl-Schwarzschild-Str 1, D-85748 Garching, Germany*
[2]*Exzellenzcluster 'Universe', Technische Universität München, Boltzmannstr 2, D-85748 Garching, Germany*
[3]*Instituto de Astrofísica de La Plata, UNLP-CONICET, Paseo del Bosque s/n, 1900 La Plata, Argentina*
[4]*Facultad de Ciencias Astronómicas y Geofísicas, UNLP, Paseo del Bosque, FWA, B1900, La Plata, Buenos Aires, Argentina*

Accepted 2020 February 3. Received 2020 January 28; in original form 2019 March 14

ABSTRACT

The treatment of convective boundaries remains an important source of uncertainty within stellar evolution, with drastic implications for the thermally pulsing stars on the asymptotic giant branch (AGB). Various sources are taken as motivation for the incorporation of convective boundary mixing (CBM) during this phase, from s-process nucleosynthesis to hydrodynamical models. In spite of the considerable evidence in favour of the existence of CBM on the pre-AGB evolution, this mixing is not universally included in models of TP-AGB stars. The aim of this investigation is to ascertain the extent of CBM, which is compatible with observations when considering full evolutionary models. Additionally, we investigate a theoretical argument that has been made that momentum-driven overshooting at the base of the pulse-driven convection zone should be negligible. We show that, while the argument holds, it would similarly limit mixing from the base of the convective envelope. On the other hand, estimations based on the picture of turbulent entrainment suggest that mixing is possible at both convective boundaries. We demonstrate that additional mixing at convective boundaries during core-burning phases prior to the thermally pulsing AGB has an impact on the later evolution, changing the mass range at which the third dredge-up and hot-bottom burning occur, and thus also the final surface composition. In addition, an effort has been made to constrain the efficiency of CBM at the different convective boundaries, using observational constraints. Our study suggests a strong tension between different constraints that makes it impossible to reproduce all observables simultaneously within the framework of an exponentially decaying overshooting. This result calls for a reassessment of both the models of CBM and the observational constraints.

Key words: stars: AGB and post-AGB.

1 INTRODUCTION

The treatment of mixing at convective boundaries presents a challenge which, despite the advent of 3D hydrodynamical simulations (Hurlburt et al. 1994; Freytag, Ludwig & Steffen 1996; Herwig et al. 2007; Baraffe et al. 2017), has proven to be a persistent source of uncertainties in 1D stellar evolution models. This is a fact which can become especially relevant when considering the evolution during the thermally pulsing asymptotic giant branch (TP-AGB), where boundaries at the edge of convective zones are known to play an important part in governing many important properties and observables of these stars (Herwig et al. 1997; Herwig 2005), such as third dredge-up (TDU) and the initial–final mass relation (IFMR). Certainly, it has been seen in hydrodynamic simulations (Freytag et al. 1996; Herwig et al. 2007; Meakin & Arnett 2007; Mocák et al. 2009; Baraffe et al. 2017; Pratt et al. 2017) that the strict Schwarzschild boundary, as implemented in 1D stellar evolution codes, simply does not appear in the form of a composition discontinuity in a spherically symmetric manner when it comes to multidimensional models.

Common ways of including additional mixing at convective boundaries are either the extension of the fully mixed convective region by a fraction of the local pressure scale height (e.g. Schaller et al. 1992) or the inclusion of an exponentially decaying velocity profile (e.g. Herwig et al. 1997). While it is well established (Maeder & Meynet 1991; Stothers & Chin 1992; Schroder, Pols & Eggleton 1997; Ekström et al. 2012) that some additional mixing is required from convective cores on the upper main sequence, it is not always the case that models produced for the TP-AGB (such as for yields or evolutionary tracks) include significant, or any, convective boundary mixing (CBM) from convective cores during the previous evolution (Karakas & Lattanzio 2007; Cristallo et al. 2009). One aspect of this paper is to focus on this pre-AGB treatment of CBM, to ascertain whether this is having a significant effect on the models which are then produced. This is of relevance

★ E-mail: mmiller@fcaglp.unlp.edu.ar

given the output from these grids of models are utilized by the wider astrophysics community. Additionally, the application of the intensity of CBM calibrated from core hydrogen burning (CHB) stars to all convective boundaries can lead to results which are in tension with observations when applied to all boundaries during the TP-AGB evolution. This has been shown to be the case for the stellar evolution codes used here (Weiss & Ferguson 2009; Andrews et al. 2015; Miller Bertolami 2016), and provides an additional motivation for examining the influence of additional mixing at the various convective boundaries. However, it is also not as simple as preventing any CBM during the TP-AGB phase, as the existence of carbon stars (C-stars) and the abundances of the PG1159 post-AGB stars provide strong evidence that CBM is indeed necessary. On the theoretical side, Lattanzio et al. (2017) pointed out that traditional, momentum-based overshooting cannot be the cause of additional CBM at the base of the pulse-driven convection zone (PDCZ). However, as presented by Meakin & Arnett (2007) CBM in phases of high thermal imbalance, such as the thermal pulses, might take the form of turbulent entrainment. We explore both arguments in this work.

The aim of this paper is to test the impact of pre-AGB CBM on TP-AGB models, and to assess the calibration of TP-AGB CBM through the use of the GARching STellar Evolution Code (GARSTEC; Weiss & Schlattl 2008) and the La Plata stellar evolution code (LPCODE, e.g. Miller Bertolami 2016), and thereby to improve stellar models in this evolutionary phase. To begin with, Section 2 discusses the treatment of CBM in our stellar evolution codes and presents the main convective boundaries in low-mass stellar evolution. A discussion of the argument presented in Lattanzio et al. (2017) together with an exploration of the possibility of CBM by turbulent entrainment then follows in Section 3. Sections 4 and 5 then presents our numerical experiments and discusses the implication for additional mixing at different convective boundaries and the possibility of constraining CBM by means of various observables. Finally, Section 6 ends the paper with some concluding remarks.

2 CONVECTIVE BOUNDARY MIXING

Traditionally referred to as overshooting, CBM has become a more commonly used term to account for the uncertainty about the mechanism responsible for such mixing and to acknowledge that it may not, in all cases, be momentum-based overshooting. In GARSTEC and LPCODE, CBM is treated diffusively, according to the description of Freytag et al. (1996), where the diffusion constant at a distance z from the convective boundary is given by

$$D(z) = D_0 \exp\left(\frac{-2z}{f_{\rm CBM} H_{\rm P}}\right), \quad (1)$$

where $f_{\rm CBM}$ is a free parameter that can be different at each convective boundary and D_0 is the value of the diffusion constant close to the convective boundary, derived from the convective velocity. Within mixing length theory (MLT) D_0 is exactly zero by definition at the formal convective border; therefore, different codes define its value in different ways: The GARSTEC version used for this work, adopts D_0 as the value of D at the convective grid point next to the formal convective boundary, while in LPCODE D_0 is defined as the mean value within $0.1H_{\rm P}$ of the formal convective boundary. In addition to D_0, a cut-off value needs to be implemented in stellar evolution codes. This cut-off value is taken as $D^{\rm cut\text{-}off} = 10^{-20} D_0$ ($D^{\rm cut\text{-}off} = 10^{-10} D_0$) in GARSTEC (LPCODE).

It is very difficult to determine how much additional mixing is likely needed in stellar evolution models at different convective boundaries and as such a variety of methods are used for current TP-AGB evolutionary models. These range from nucleosynthesis arguments for the extent of CBM necessary to reproduce the ^{13}C pocket below the convective envelope (CE) to hydrodynamical simulations or AGB/post-AGB observables that need to be fitted by a given choice of the CBM intensity. These arguments are subsequently reviewed here.

2.1 Core hydrogen burning

There is considerable evidence for additional mixing for CHB stars on the upper main sequence, with a consensus that it extends to roughly 20 per cent of the local pressure scale height (Schaller et al. 1992; Herwig et al. 1997; Weiss & Ferguson 2009; Ekström et al. 2012; Miller Bertolami 2016). This is seen by the ability to reproduce the observations of the main sequence stars in open clusters (Maeder & Meynet 1991; Stothers & Chin 1992; Schroder et al. 1997) and eclipsing binaries (Claret 2007; Stancliffe et al. 2015; Higl & Weiss 2017).

2.2 Core helium burning

CBM at the He-burning core can be physically motivated (Castellani, Giannone & Renzini 1971; Castellani et al. 1985). Castellani et al. (1971) showed that any extension of the convective boundary beyond its formal value as given by the simple (and naive, see Gabriel et al. 2014) application of the Schwarzschild criterion is expected to increase the C abundance of the neighbouring layers. This in turn leads to an increase in their opacity, and consequently of $\nabla_{\rm rad}$, and thus to an even larger convective core. The increase of the size of the convective core moves the convective boundary, and CBM, even further until $\nabla_{\rm rad}$ equals the local value of the adiabatic gradient $\nabla_{\rm ad}$. In fact, it can be argued that a correct application of the Schwarzschild criterion should always guarantee that neutral buoyancy (i.e. $\nabla_{\rm rad} = \nabla_{\rm ad}$) is attained at both sides of the convective border (Gabriel et al. 2014; Salaris & Cassisi 2017). In addition to this self-driving mechanism, the subsequent He-core burning later gives rise to the appearance of splittings in the formal convective core that can be modelled as a partially mixed region, where neutral buoyancy is attained (Castellani et al. 1985). The inclusion of some minor CBM in stellar evolution models allows the convective zones to stay connected, and although details in the final chemical profiles keep a record of the exact method adopted for computing mixing beyond the formal convective boundary, under moderate assumptions for CBM all algorithms lead to similar sizes in the final He-burning cores (Bossini et al. 2015; Constantino et al. 2015; Constantino, Campbell & Lattanzio 2017; De Gerónimo et al. 2019).

Asteroseismic studies of core helium burning (CHeB) stars support the existence of the processes mentioned above (Charpinet et al. 2011; Constantino et al. 2015), and might even help to select a preferred algorithm (Bossini et al. 2015). The evidence from star counts (Constantino et al. 2016) also seems to suggest that the naive implementation of the Schwarzschild Criterion in CHeB wrongly estimates the size of He-burning cores (as pointed out by Gabriel et al. 2014).

Numerical experiments with LPCODE show (see fig. 2 of De Gerónimo et al. 2019) that, as long as $f_{\rm CHeB}$ is included and kept within a moderate range ($0 < f \lesssim 0.035$) the evolution of all relevant quantities remains almost unchanged. Due to the lack of very tight constraints and the fact that under moderate assumptions for CBM in the He-burning core all algorithms lead to similar sizes in the

convective cores (Bossini et al. 2015; Constantino et al. 2015; Constantino et al. 2017; De Gerónimo et al. 2019), it is common practice to take the same calibration as in the CHB phase and to apply it to the CHeB as well (e.g. Weiss & Ferguson 2009; Miller Bertolami 2016; Jones et al. 2016; Ritter et al. 2018).

2.3 Convective envelope and pulse-driven convective zone

The boundaries of these convective zones are best considered together, given the inevitable connection between the two when considering the TP-AGB. It is already known that stellar evolution codes tend to require some form of additional mixing on the TP-AGB in order to achieve sufficient dredge-up to reproduce statistics from carbon star counts (e.g. from Girardi & Marigo 2007), at the necessary mass and metallicity (Herwig et al. 1997; Weiss & Ferguson 2009; Miller Bertolami 2016). However, it has also been shown that the inclusion of the value for $f_{\rm CBM}$ as calibrated by upper main-sequence stars at all convective boundaries (e.g. in Weiss & Ferguson 2009) results in such efficient TDU that core growth is suppressed during the TP-AGB, leading to an IFMR that is in tension with observations, the predicted final mass being too low by ~ 0.1–$0.2\,{\rm M}_{\odot}$ for initial masses in the range ~ 2–$4\,{\rm M}_{\odot}$ (Salaris et al. 2009; Cummings et al. 2018; El-Badry, Rix & Weisz 2018).

CBM below the CE plays two different roles. On the one hand, even the inclusion of an inefficient CBM at the bottom of the CE is known to enhance TDU during the TP-AGB (Herwig 2000). On the other hand, CBM below the CE is required to enrich sufficiently the partially mixed regions in H and C to ensure the formation of a ^{13}C pocket. The radiative burning of this ^{13}C pocket is the main source of neutrons for the formation of heavy elements through slow neutron captures (s-process nucleosynthesis). Attempts to calibrate the value of $f_{\rm CE}$ by different means have lead to contradictory results. While some authors have found that very intense CBM might even be required to match the O-rich to C-rich transition luminosity of AGB stars in Magellanic Cloud clusters (Kamath, Karakas & Wood 2012), others concluded that such intense CBM at the bottom of the CE cannot be reconciled with the ratios of C- and M-stars in the Magellanic Clouds' Globular Clusters or the IFMR (Miller Bertolami 2016). In fact, several recent works do not include any CBM at all at the bottom of the CE for the computation of their model grids (i.e. $f_{\rm CE} = 0$, e.g. Karakas 2014; Miller Bertolami 2016). This is in stark contradiction to what is necessary to reproduce s-process abundances. From a calibration of the ^{13}C pocket, Cristallo et al. (2009) found an intensity of CBM at the bottom of the CE that corresponds to a value of $f_{\rm CE} \sim 0.2$. Similarly, from the partially mixed mass required at the bottom of the CE given by Lugaro et al. (2003) and Herwig, Langer & Lugaro (2003), Ritter et al. (2018) derived a value of $f_{\rm CE} = 0.126$. Note that in all these papers the diffusive approach for CBM was used.

Regarding CBM at the PDCZ, a combined 2D/3D study by Herwig et al. (2007) tried to focus specifically on the TP-AGB boundaries. The result of which suggested that the boundary at the base of the PDCZ could be approximated by two exponential decays, the first beginning inside the convective region with a value of $f_{\rm PDCZ} = 0.01$, and a second outside the convective zone with a value of $f_{\rm PDCZ} = 0.14$. The top boundary was more simply modelled by a single decay, with a value of $f_{\rm CBM} = 0.1$. However, in later works Ritter et al. (2018) suggest that a value of $f_{\rm PDCZ} = 0.008$ is motivated by the same simulations of Herwig et al. (2007).

At least some additional mixing appears to be required from the observations of post-AGB stars (specifically those referred to as PG 1159 stars) which are believed to display at the photosphere the final intershell abundances of TP-AGB stars (Herwig et al. 1999). A constraint of $f_{\rm PDCZ} = 0.01$–0.03 was suggested from a preliminary investigation carried out by Herwig (2000). These results were extrapolated from a few thermal pulses of a single evolutionary model, but later explorations (Miller Bertolami 2015, 2016) suggest a lower value, $f_{\rm PDCZ} \sim 0.005$–0.0075.

3 CHARACTERIZING CONVECTIVE BOUNDARIES ON THE TP-AGB

3.1 A buoyancy argument and momentum-driven overshoot

Besides the observational and hydrodynamical constraints, some physical arguments can be constructed to understand the situation of CBM during the TP-AGB.

Thermal pulses on the AGB develop when the He-burning shell becomes geometrically thin and the gravothermal specific heat becomes positive, leading to a thermal runaway [see section 34.2 in Kippenhahn, Weigert & Weiss (2012) for a detailed discussion of the process]. As a consequence, during a thermal pulse temperature rises, leading to an increase by several orders of magnitude of the He-burning luminosity, which reaches typical values of $L_{\rm He} \gtrsim 10^7\,{\rm L}_{\odot}$. This leads to the development of a convective zone (the PDCZ) that extends outwards from the temperature peak. In addition of the creation of the PDCZ itself, the thermal pulse also creates a significant temperature inversion at the lower convective boundary of the PDCZ. An argument has been made (Lattanzio et al. 2017) that this temperature inversion would act so strongly against any convective eddy which may emerge from the bottom of the convective zone, that it would be impossible for any momentum-driven overshooting to cover any appreciable distance. The basic physical argument is outlined in Lattanzio et al. (2017), and it focuses on the buoyancy acting against a convective element which travels beyond the formal convective boundary. By considering a convective element of density $\rho_{\rm e}(r)$ at the base of the convective zone, moving downwards adiabatically, they compute the deceleration of the element until it stops. Then the distance $d_{\rm pen} = |r_1 - r_0|$ travelled beyond the formal convective boundary (at r_0) is given by

$$\frac{1}{2}v_0^2 = \int_{r_0}^{r_1} g(r)\left[\frac{\rho(r) - \rho_{\rm e}(r)}{\rho_{\rm e}(r)}\right]{\rm d}r, \tag{2}$$

where v_0 is a 'typical turbulent velocity' near the convective boundary. It should be mentioned that the adiabatic approximation is very accurate for convective elements in deep convective zones such as the PDCZ. Also at the bottom of the CE of red giants the adiabatic approximation is good, as discussed by Viallet et al. (2015). This is reflected by the large Pecléc numbers (*Pe*) of convective elements in both the PDCZ and the CE (see Table 1). Above argument has been applied to models calculated with GARSTEC and LPCODE to investigate its relevance. At variance with what is done by Lattanzio et al. (2017), we estimate the value of v_0 near the edge of the convective zone (we take v_0 as the mean value within $0.1H_{\rm P}$ of the convective boundary) instead as the maximum value within the convective zone. This leads in our case to values of $d_{\rm pen}$ lower by a factor of a few in comparison with those estimated by Lattanzio et al. (2017).

Table 1 shows characteristic numbers during the 6th and 13th thermal pulses of an initially $M_{\rm i} = 3\,{\rm M}_{\odot}$ sequence ($Z_{\rm ZAMS} = 0.01$) computed with LPCODE. Models are taken from Miller Bertolami (2016) but with CBM inhibited for this experiment. As shown in Table 1, according to the criterion presented by Lattanzio et al.

Table 1. Characteristic values of the turbulent velocity $v_{\rm MLT}$, Péclet Number Pe, penetration distance $d_{\rm pen}$, distance entrained during the duration of the flash $d_{\rm ent}$, and time-scale required to entrain a distance equal to the local pressure scale height $\tau^{1H_{\rm P}}$, for different convective boundaries and during the 6th and 13th thermal pulses of an initially $M_i = 3\,{\rm M}_\odot$ sequence ($Z_{\rm ZAMS} = 0.01$) computed with LPCODE (Miller Bertolami 2016); see the text for additional explanations.

Convective border	$v_{\rm MLT}$ (cm s^{-1})	Pe	$d_{\rm pen}$ (cm, $H_{\rm P}$)	$d_{\rm ent}/H_{\rm P}^0$	$\tau^{1H_{\rm P}}$ (yr)
6th TP: $\log L_{\rm He}^{\rm max} = 6.85$, $\tau^{\rm peak} = 2.5$yr					
Bottom PDCZ	2.25×10^5	10^7	3950, 2.2×10^{-5}	0.16	25
Bottom CE (Max. $L_{\rm He}$)	8×10^4	500–3000	2.5×10^7, 3.3×10^{-3}	0.37	68
Bottom CE (Max. depth CE)	4.3×10^5	1000–10 000	1.6×10^6, 5.9×10^{-4}	–	4.1
13th TP: $\log L_{\rm He}^{\rm max} = 8.23$, $\tau^{\rm peak} = 0.127$yr					
Bottom PDCZ	6×10^5	10^7–10^8	3500, 2.2×10^{-5}	0.11	1.4
Bottom CE (Max. $L_{\rm He}$)	9.6×10^4	700–2000	2×10^7, 3.3×10^{-3}	0.17	32
Bottom CE (Max. depth CE)	5.7×10^5	350–4000	1.3×10^6, 3.5×10^{-4}	–	1.9

(2017) convective elements should indeed barely penetrate into the neighbouring stable regions. The estimated penetrated distance is of the order of $10^{-5} \times H_{\rm P}$ for the lower boundary of the PDCZ and somewhat larger, but still very small at the bottom of the CE (around $10^{-4} \times H_{\rm P}$ at the point of maximum penetration of the CE).

3.2 Stiffness of the convective boundary: $Ri_{\rm B}$

The previous dynamical argument suggests that no momentum-driven overshoot at the bottom of any convective zone should be expected during the TP-AGB. However, as noted by Viallet et al. (2015) in quick phases of high thermal imbalance the proper regime of CBM might correspond to that of turbulent entrainment as defined by Meakin & Arnett (2007). In the case of turbulent entrainment, turbulence diffuses into the stable regions leading to a progressive advance of the whole border of the turbulent region. Consequently, while the argument discussed above might suggest the absence of overshooting at TP-AGB convective boundaries, it might be far from the actual physical process driving CBM in these stars. According to Meakin & Arnett (2007), the speed $u_{\rm E}$ at which the turbulent border advances into the neighbouring stable layers is given by

$$u_{\rm E} = \sigma\, A\, Ri_{\rm B}^{-n}, \tag{3}$$

where $Ri_{\rm B}$ is the bulk Richardson number and σ the rms of velocities at the turbulent border. A fit to numerical simulations of oxygen-shell burning and core-hydrogen burning by Meakin & Arnett (2007) suggests that $\log A = 0.027 \pm 0.38$ and $n = 1.05 \pm 0.21$, in agreement with theoretical arguments and other numerical experiments. For all practical purposes this means that $u_{\rm E} \simeq \sigma/Ri_{\rm B}$. The bulk Richardson number is a measure of the stiffness of the boundary region, defined as

$$Ri_{\rm B} = \frac{\Delta b\, L}{\sigma^2}, \tag{4}$$

where L is a length-scale of the turbulent motions and Δb is the buoyancy jump across the transition. Here, the relative buoyancy $b(r)$ is defined by

$$b(r) = \int_{r_0}^{r} N^2 {\rm d}r, \tag{5}$$

where N is the local angular buoyancy frequency. Unfortunately, in stellar evolution models the computation of Δb cannot be performed as the width of transition region between stable and turbulent layers is undefined.

However, we can estimate a typical time-scale that it would take the boundary to reach a given radius r beyond the convective boundary as

$$\tau(r) = \frac{|r - r_0|}{u_{\rm E}(r)} \simeq \frac{|r - r_0| b(r) L}{\sigma^3}, \tag{6}$$

where we have taken r_0 as the location of the formal convective boundary in the stellar evolution model so that $b(r) = \Delta b$. By estimating the length-scale of turbulence as the mixing length at the convective border ($L = \alpha_{\rm MLT} H_{\rm P}^0$), and σ as the MLT velocity near the convective boundary (again we take v_0 as the mean value within $0.1\,H_{\rm P}^0$ of the convective boundary), we can compute a value for $\tau(r)$. In this way, we can now estimate the entrainment distance ($d_{\rm ent}$) of the turbulent border by equating the $\tau(r)$ with a typical duration of the thermal pulse $\tau_{\rm peak}$. In what follows, we define $\tau_{\rm peak}$ as the time spent by the He-burning luminosity within one order of magnitude of its maximum value.[1] In Table 1, we show the entrainment distances during two thermal pulses of an initially $M_i = 3\,{\rm M}_\odot$ star [$Z = 0.01$, taken from Miller Bertolami (2016), but with CBM inhibited for this experiment]. At variance with the previous estimation, this consideration suggests that the bottom of the PDCZ is able to penetrate a distance of $d_{\rm ent} \gtrsim 0.1 H_{\rm P}^0$ into the stable layers. If this is the case, then CBM at the bottom of the PDCZ is not only possible but also significant, and should be included in stellar evolution models.

Additionally, we show in Table 1 the time estimate ($\tau^{1H_{\rm P}}$) for the entrainment to penetrate a distance of $d_{\rm ent} = 1 H_{\rm P}^0$ both at the bottom of the PDCZ and the CE. While in the case of the PDCZ this time-scale is about 10 times the duration of the peak of He-burning, in the case of the bottom of the CE the time-scale is shorter than the duration of the CE being at maximum depth after the thermal pulse (which is of ∼120 and ∼320 yr for the 3rd and 13th thermal pulses, respectively). This can be taken as a hint that CBM at the bottom of the CE at the time of maximum depth of the CE (which is responsible for the later formation of the ^{13}C pocket in AGB stars) is expected to be large. From these considerations we conclude that CBM at the bottom of the CE is much more efficient than at the bottom of the PDCZ. However, a word of caution is in order regarding the limitations of these estimations: While convection close to the border of the PDCZ has Péclet numbers[2] of the order

[1] Note that as soon as the He-burning luminosity drops significantly, also the convective velocities drop and the formal convective boundary recedes.

[2] Throughout this section we use the effective value of the Péclet number proposed by Viallet et al. (2015) for stellar evolution models within the MLT theory of convection, which is $Pe = 3D/\chi$ where D and χ stand for the coefficients for chemical mixing and thermal diffusion, respectively.

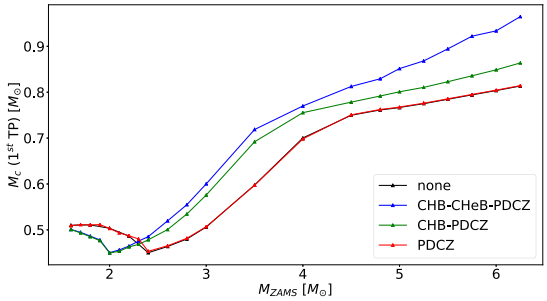

Figure 1. The core mass at the first thermal pulse as a function of initial mass for sequences computed with CBM included at different convective boundaries. All sequences correspond to initial metallicities of $Z = 0.02$. Note the shift in $\sim 0.4\,M_\odot$ in the progenitor mass when CBM is included in the convective cores.

of $Pe \gtrsim 10^7$ and the entrainment law of Meakin & Arnett (2007) can thus be expected to be valid, values at the bottom of the CE are typically more than four orders of magnitude smaller (see Table 1). As a consequence, if the velocity drops exponentially outside the formal convective border, it is expected that CBM beyond the formal convective boundary will stop to be adiabatic already close to the boundary, and the entrainment picture of Meakin & Arnett (2007) will stop to be valid.

4 NUMERICAL EXPERIMENTS

Calculations in Sections 4 and 5 were performed mostly using GARSTEC (Weiss & Schlattl 2008; Weiss & Ferguson 2009; Wagstaff & Weiss 2018) and, when explicitly noted, also LPCODE (Miller Bertolami 2016). Models presented in Section 6 were computed with LPCODE. The physics and numerics adopted in this work are consistent with those described in the above papers and the details can be found there. The exception to this is the main focus of study of this paper, i.e. the efficiency of CBM at different stages of the evolution. For the sake of completeness we summarize some of the most important ingredients adopted for this work. Both GARSTEC and LPCODE sequences where computed with an Eddington grey atmosphere throughout the evolution. Both codes adopt high-temperature radiative opacities from the OPAL project (Iglesias & Rogers 1996), and low-temperature molecular opacities from Wichita State Alexander & Ferguson molecular opacity tables (Ferguson et al. 2005; Weiss & Ferguson 2009) for solar-like as well as for C-rich mixtures. Conductive opacities are included in this version of GARSTEC (Weiss & Ferguson 2009) following Itoh et al. (1983) while LPCODE adopts the conductive opacities of Cassisi et al. (2007). The neutrino emission by plasma processes from the degenerate core of red giants is adopted in both codes according to Haft, Raffelt & Weiss (1994). For the equation-of-state (EOS) GARSTEC sequences were computed with the Irwin's EOS (Cassisi, Salaris & Irwin 2003) in the form of pre-calculated tables, while LPCODE sequences adopt the updated `EOS_2005` version of the OPAL EOS (Rogers, Swenson & Iglesias 1996). When outside the parameter range of modern tabular EOS both codes rely on a Saha-type EOS. Regarding the treatment of convective energy transport both codes rely on the MLT of convection as described in Kippenhahn et al. (2012). The free parameter $\alpha_{\rm MLT}$ was taken as 1.75 and 1.822 in GARSTEC and LPCODE, respectively. Mass-loss has been included in similar fashion as in previous works. GARSTEC sequences were computed with a mixture of Reimers (1975), Wachter et al. (2002), and van Loon et al. (2005) prescriptions as described in Weiss & Ferguson (2009), while LPCODE sequences rely on a mixture of Schröder & Cuntz (2005), Groenewegen et al. (1998), and Groenewegen et al. (2009), as described in Miller Bertolami (2016), where we have explored current constraints on CBM during CHB, CHeB, mixing from the lower boundary of a CE, and from the convective boundaries of PDCZs.

GARSTEC models presented in Sections 4 and 5 were calculated for two compositions, taking $Z = 0.02$ and $Y = 0.28$ for the solar case and $Z = 0.008$ and $Y = 0.25$ for an LMC comparison. Both set of models take the abundances of Grevesse & Noels (1993). TP-AGB models were computed until the computations failed to converge due to numerical instabilities just before the end of the TP-AGB (Weiss & Ferguson 2009; Lau et al. 2012). The values for the efficiency of CBM in the following sections and experiments (namely, $f_{\rm CHB}$, $f_{\rm CHeB}$, $f_{\rm CE}$, and $f_{\rm PDCZ}$) have been chosen to encompass the values derived by previous authors and discussed in Section 2.

4.1 Convective cores

The size of convective cores present in the pre-AGB stages of evolution, during CHB and CHeB, determine the mass of the H- and He-free cores at the beginning of the TP-AGB. As a consequence, CBM at these convective cores can be expected to play a role during the TP-AGB. Exploring the impact of CBM during CHeB and CHB stages on the TP-AGB evolution is the purpose of this section. Here, we compute models with GARSTEC for different initial masses that include, or exclude, CBM during the CHB ($f_{\rm CHB} = 0.0174$) and/or the CHeB ($f_{\rm CHeB} = 0.0174$) and then follow the subsequent TP-AGB evolution. During the TP-AGB phase, CBM was included only at the PDCZ ($f_{\rm PDCZ} = 0.0075$, $f_{\rm CE} = 0$), with the exception of an additional comparison sequence that was computed without CBM at all convective boundaries. These sequences are then labelled 'None', 'CHB-PDCZ', 'CHB-CHeB-PDCZ', and 'PDCZ' according to the convective zones at which CBM was included. Note that the sequences label-led 'CHB-CHeB-PDCZ' have the same choice of $f_{\rm CBM}$-parameters as the model grids computed by Miller Bertolami (2016).

4.1.1 *At the onset of the TP-AGB*

Fig. 1 shows the mass of the H-free core ($M_{\rm c}^{\rm TP1}$) at the moment of the first thermal pulse (i.e. the beginning of the TP-AGB phase) for stellar evolution sequences computed under different assumptions. Note that models with CBM only at the PDCZ boundaries and models with no CBM at any convective boundary are identical before the TP-AGB. The mass of the H-free core (HFC) provides a very clear indication of how CBM before the TP-AGB influences the behaviour on the TP-AGB.

The first thing that becomes apparent between models with and without CBM during the core-burning stages is the shift in the minima of $M_{\rm c}^{\rm TP1}$ as a function of the initial mass $M_{\rm ZAMS}$ (Fig. 1). This minima corresponds to the transition initial mass below (above) which helium burning commences in a degenerate (non-degenerate) core. This transition mass shifts by about $\sim 0.4\,M_\odot$ when CBM is included during the main sequence (CHB). Note that this transition mass is in no way affected by the inclusion or not of CBM during the CHeB phase (see Fig. 1). This is because it is the size of the mixed core during the CHB that defines the size of the He-core after the main sequence, and whether such core is massive enough to ignite He in a non-degenerate way. CBM at the CHeB becomes only important once stable He-core burning begins. The impact of CBM during the CHeB phase can be appreciated for higher initial mass

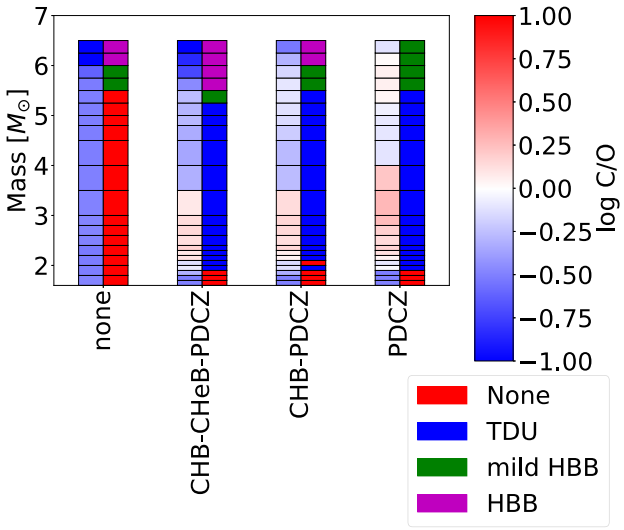

Figure 2. C/O values and classifications of TDU and HBB for sequences that include CBM at different convective boundaries. All sequences correspond to initial metallicities of $Z = 0.02$. Each set of models is represented by two columns, the left of which shows the final surface C/O value (matched to the colour bar at the side) while the right-hand column shows the model classification; the initial mass is given along the vertical axis. The classification is defined as follows: red – no TDU, blue – TDU, green – mild HBB, magenta – HBB. Initial C and O abundances correspond to log C/O = −0.32 by number fraction.

models, for which the inclusion of CHeB begins to influence $M_c^{\rm TP1}$ by increasing the core mass. This effect becomes even stronger with increasing initial mass.

The overall effect of including CBM for convective cores is that models mimic the behaviour of models with larger initial masses ($\Delta M_{\rm i} \sim 0.4\,{\rm M}_\odot$), but without CBM for convective cores. This results in generally less massive cores for the low-mass stars ($M_{\rm i} \lesssim 2.5\,{\rm M}_\odot$), but more massive cores for higher initial mass. This will have a clear impact on the initial threshold masses $M_{\rm ZAMS}$ at which a star is expected to begin TDU or hot-bottom burning (HBB). Proper pre-AGB evolution is therefore important when AGB yields or AGB properties need to be linked to the initial progenitor masses, or the age of the host stellar population.

4.1.2 Third dredge-up

Still focusing on the models including CBM during convective core phases, the surface C/O values at the end of our computations can be seen in Fig. 2 as a function of initial mass, for the different combinations of boundaries where additional mixing has been applied. Alongside the final C/O value appears the classification of whether the models undergo TDU, HBB or what is here classified as mild HBB. This last category arises for models where a reduction in the carbon isotopic ratio, $^{12}{\rm C}/^{13}{\rm C}$, is observed although no significant reduction in either the C/O or C/N value occurs.

In the set of models where no additional mixing is applied, there is a lack of dredge-up in all models, although HBB still occurs for the higher mass models. In contrast, the models with mixing only applied at the PDCZ experience a significant increase in carbon due to dredge-up. The comparison between all the sets of sequences that include CBM at the PDCZ clearly shows that core size has a significant influence on HBB, as any difference arises from the initial core size as was shown in Fig. 1. This can be seen by the fact that the models with the largest cores at higher masses, CHB–CHeB–PDCZ, experience HBB at the lowest initial masses and to the greatest degree, while the CHB–PDCZ and PDCZ models undergo progressively less HBB. That the set of models with no additional mixing experience HBB to a larger extent than the PDCZ models, despite beginning with the same core size, seems to be because mixing from the PDCZ boundaries inhibits HBB, due to the increase in the helium luminosities generated.

As for TDU, it can again be seen to alter its behaviour as a result of the treatment of convective core boundaries. The similarity between the CHB-CHeB-PDCZ models and the CHB-PDCZ models for initial masses which have degenerate cores at the onset of helium burning, begins to diverge above this; the more efficient dredge-up for the latter indicates that the lower core mass results in a final model which is more carbon-rich. This pattern continues when considering the PDCZ-only models, which have a lower initial core mass at higher masses (and more efficient dredge-up), but larger cores at lower initial masses (and less efficient dredge-up). Indeed, combined with the lack of HBB in the more massive PDCZ-only set of models, it can even be observed that a 5.5 $\rm M_\odot$ model becomes carbon rich.

Overall the effect of including additional CBM during core burning phases can play a significant role in changing the outcome of TP-AGB calculations, and given the evidence in favour of the existence of CBM during the core burning stages this effect needs to be addressed. This evidence is also reinforced by the recent hints of the existence of HBB in stars with initial masses as low as $M_{\rm ZAMS} \sim 3\,{\rm M}_\odot$ (Fang et al. 2018; Henry et al. 2018; Davis et al. 2019).

The inclusion of CBM in pre-AGB stages is particularly important when trying to link the C and N abundances measured in PNe with the initial mass of the progenitor star (e.g. Henry et al. 2018; Madonna et al. 2018; Davis et al. 2019). In particular, the adoption of nucleosynthesis computations based on stellar models that do not include CBM on the upper main sequence (e.g. Cristallo et al. 2015; Karakas & Lugaro 2016), might lead to a systematic shift in the nucleosynthesis predictions as a function of the initial mass by $\sim 0.4\,{\rm M}_\odot$, see Fig. 1, with additional consequences for deriving time-scales of galactic chemical evolution.

4.2 Impact of CBM during second dredge-up

In this section, we analyse the impact of second dredge-up (2DUP) on the mass of the HFC during the subsequent TP-AGB evolution, and on the final C/O ratio. In particular, we try to assess the impact of 2DUP on the threshold for HBB. Fig. 3 shows the evolution of several sequences in which the 2DUP was computed under the assumption of different values of the CBM parameter $f_{\rm CE}$. Note that for the sake of these experiments, CBM during the main sequence, core-He burning, and TP-AGB phases was kept constant with values of $f_{\rm CHB} = 0.0174$, $f_{\rm CHeB} = 0.0174$, $f_{\rm PDCZ} = 0.0075$, and $f_{\rm CE} = 0$, respectively. Thus, our reference sequence with no CBM at the bottom of the CE corresponds to those sequences labelled as CHB-CHeB-PDCZ in Fig. 2. The right-hand panels in Fig. 3 show the evolution of the HFC (and consequently the location of the bottom of the H-rich CE) during the 2DUP and the TP-AGB. The incorporation of CBM during 2DUP produces a decrease of the HFC of a few per cent in $M_{\rm HFC}$ (up to ∼5 per cent) at the point of maximum depth, i.e. at the beginning of the TP-AGB. While this difference is not negligible it is smaller than those produced by CBM during the main sequence. This becomes clear when comparing Fig. 1 with Fig. 3: While CBM during the main sequence leads

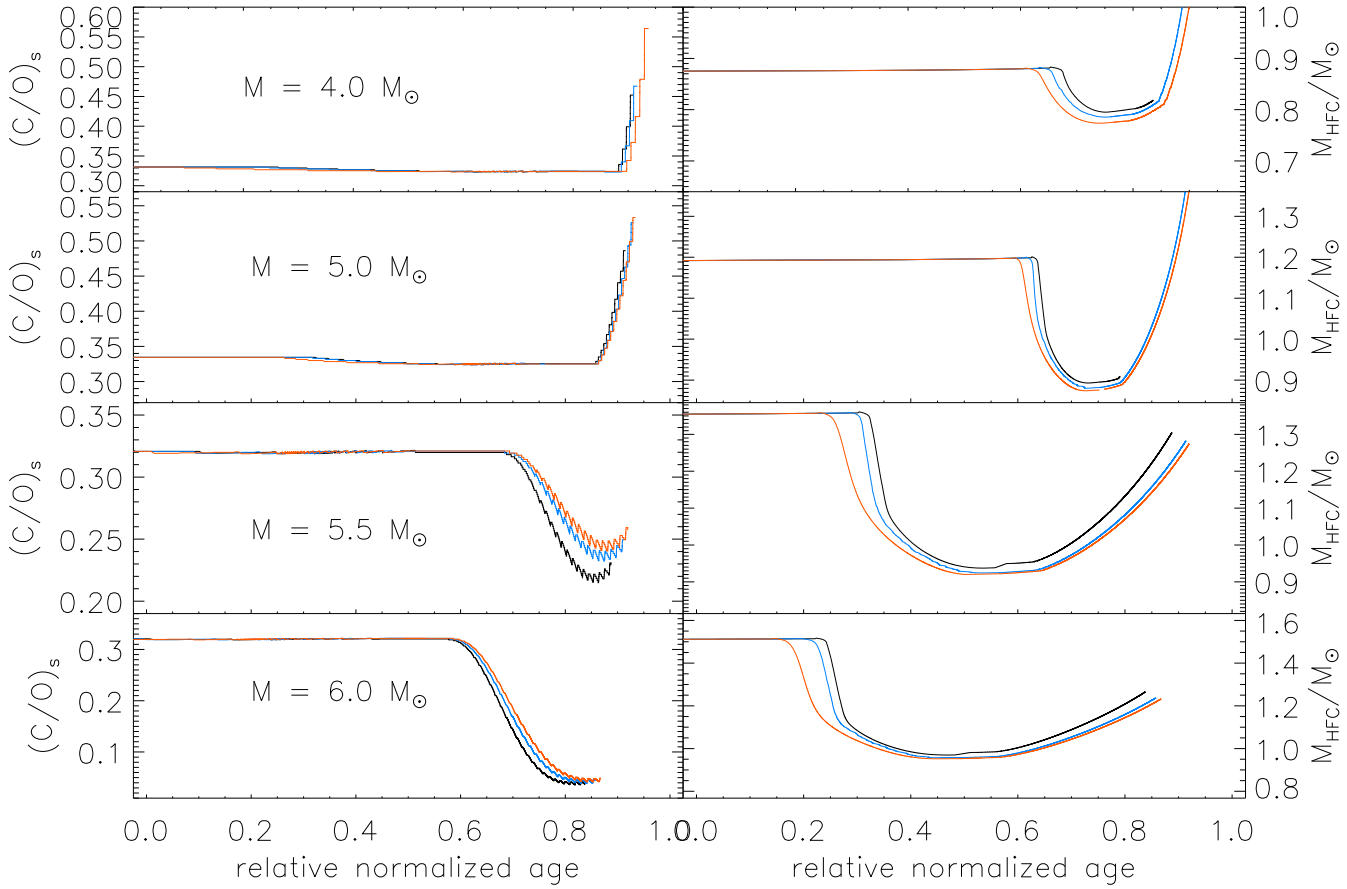

Figure 3. Impact of CBM during 2DUP on the subsequent evolution for evolutionary sequences of $M_{\rm ZAMS} = 4,\ 5,\ 5.5$, and $6\,{\rm M}_{\odot}$. The sequences shown here have been computed in all cases with $f_{\rm CHB} = 0.0174$, $f_{\rm CHeB} = 0.0174$, $f_{\rm PDCZ} = 0.0075$, $f_{\rm CE} = 0$, during the main sequence, core-He burning and TP-AGB phases, only altering the value of $f_{\rm CE}$ during the 2DUP. Left-hand panels show the change in the photospheric C/O ratio when 2DUP is computed with strong (orange, $f_{\rm CE} = 0.126$), moderate (blue, $f_{\rm CE} = 0.0174$), or no CBM ($f = 0$). Right-hand panels show the evolution of the HFC for the same evolutionary sequences (in mass coordinate). The relative normalized age plotted in the x-axis is defined in such a way that it covers the relevant period between the end of CHeB and the end of the computation, in order to allow a direct comparison for all four mass values. For each mass value this 'relative normalized age' is identical for all three cases of $f_{\rm CE}$. All sequences correspond to initial metallicities of $Z = 0.02$.

to differences of almost 20 per cent in the size of the HFC, CBM at the CE during the 2DUP leads to initially only a change of a few per cent, and even after the TP-AGB the impact of CBM during the 2DUP leads to differences of not more than 10 per cent in the HFC size. Note that in these experiments CBM is included at the bottom of the CE only during 2DUP, but not during the TP-AGB. Changes introduced by CBM during the 2DUP are also small regarding the impact of CBM during the 2DUP on the C/O ratio, and in particular of the development of HBB. As shown in the left-hand panels of Fig. 3, HBB is active for stars with $M_{\rm i} \gtrsim 5.5\,{\rm M}_{\odot}$, noticeable by the continuous decrease in the C/O ratio, regardless of the assumption about CBM during the 2DUP. This is in contrast to the dependence of HBB to the inclusion of CBM during the CHB, CHeB, and PDCZ shown in Fig. 2, where the intensity of HBB changes from no-HBB to mild HBB and full HBB as a consequence of CBM in those stages. Also, the left-hand panels in Fig. 3 show that TDU and the evolution of C/O during the TP-AGB are only slightly affected by the occurrence of any CBM during the 2DUP event.

We conclude from this experiment that CBM during the 2DUP leaves only a minor impact on the structure of the future TP-AGB star, and leads to changes in 3DUP and HBB smaller than those produced by the inclusion of CBM at other stages of the evolution like the core H- and He-burning, and He-shell flashes on the TP-AGB.

4.3 Impact of CBM during the TP-AGB on third dredge-up efficiency

An investigation performed by Herwig (2000) showed the variation in the TDU efficiency[3] λ as a function of mixing efficiency at the different convective boundaries. A similar approach is taken here to determine the relative importance of the different convective boundaries for the TDU during a single thermal pulse. Each calculation begins with the same initial model prior to that thermal pulse, and is evolved further with the indicated mixing efficiency applied at the various boundaries.

The model taken for this investigation is from a 3 $\rm M_{\odot}$ evolutionary sequence just prior to the 11th thermal pulse where additional mixing from both the hydrogen and helium burning cores was included, but no CBM treatment during the TP-AGB was applied prior to the thermal pulse. It is worth determining whether both convective boundaries of the PDCZ, upwards (U) and downwards (D), are influential or not. Fig. 4 shows the TDU efficiency λ for sets of models calculated independently of each other, with values

[3]The TDU efficiency is defined as the ratio between the mass of material dredged-up from the core to the mass by which the core grew during the preceding interpulse phase, given by $\lambda = M_{\rm DU}/M_{\rm growth}$.

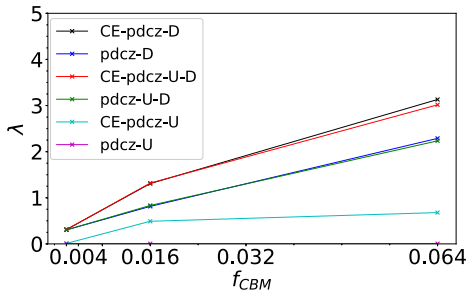

Figure 4. Dredge-up efficiency λ as a function of convective boundary mixing efficiency $f_{\rm CBM}$, for a single thermal pulse of a 3 $M_\odot$ model. Each line represents the inclusion of CBM at the different boundaries indicated. All sequences correspond to initial metallicities of $Z = 0.02$.

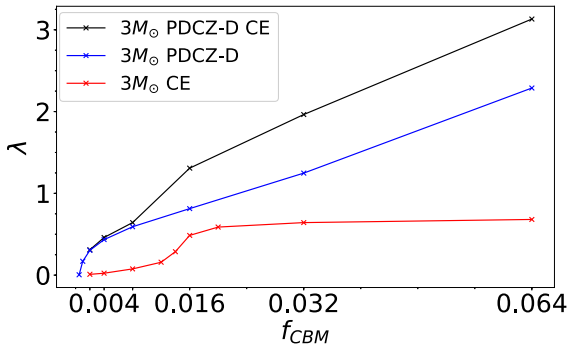

Figure 5. Dredge-up efficiency λ as a function of convective boundary mixing efficiency $f_{\rm CBM}$, for a single thermal pulse of a 3 $M_\odot$ model. Each line represents the inclusion of CBM at the different boundaries indicated. Note that CBM was included in all models during previous core-burning phases.

for the parameter $f_{\rm CBM} = [0.002, 0.016, 0.064]$ for combinations of convective boundaries at the CE, PDCZ-U, and PDCZ-D. In each case, it can be seen that mixing upwards from the PDCZ has almost no effect, apart from the cases with high $f_{\rm CBM}$ values in conjunction with mixing from the CE where it alters the outcome to a small degree. This is the boundary which is expected to have no influence on the evolution, and as this appears to be the case in the initial testing, it is from this point on ignored.

The mixing at the base of the PDCZ influences the dredge-up through an increase in the helium burning luminosity, a result of mixing additional fuel from the intershell region into the helium burning shell. This additional energy release is immediately absorbed by the layers above the He-burning shell which consequently cool and expand. This additional expansion and cooling of these layers, among which are those layers at the base of the CE, creates more favourable conditions for TDU as it increases the radiative gradient, according to $\nabla_{\rm rad} \propto T^{-4}$ (Herwig 2000).

A combination of the PDCZ-D and CE boundaries was then calculated for $f_{\rm CBM} = [0.002, 0.004, 0.008, 0.016, 0.032, 0.064]$, with additional values for the CE-only ($f_{\rm CE} = [0.012, 0.014, 0.020]$) and PDCZ-only cases ($f_{\rm PDCZ} = [0.0005, 0.001]$). The resulting TDU efficiencies are presented as λ in Fig. 5. The red line in this figure represents models which have $f_{\rm CBM}$ applied only to the CE, blue lines stand for PDCZ-D and black one for the combined CE-PDCZ-D. For models where only the CE boundary is active, additional computations were included in order to resolve the sudden increase of $\lambda(f_{\rm CMB})$ at about $f_{\rm CBM} \sim 0.016$.

Qualitatively, there appears to be a limiting value for λ in the case of mixing from the CE only, as was also observed by Herwig (2000). While in this paper it appeared as an almost 'on-off' switch, we find a limited range of $f_{\rm CBM}$ where the CE becomes relevant. Additionally, the approximate limiting value of $\lambda \simeq 0.7$ is quantitatively comparable to that in Herwig (2000), although this could be coincidental, given the different initial models, methodology and operating codes.

Focusing instead on the blue line, representing the models with only PDCZ-D, it can be seen that the base of the PDCZ already begins to have an influence on the TDU at the lower values of $f_{\rm PDCZ}$ and, from $f_{\rm PDCZ} = 0.004$ onwards, has a linearly increasing effect on λ to a fairly reasonable approximation. This behaviour is also observed in the models calculated by Herwig (2000), and has fairly strict observational limits making it unnecessary to consider higher $f_{\rm CBM}$ values in order to find out whether this trend could continue indefinitely.

It is also interesting to note that the behaviour of the two convective boundaries do not appear to be coupled, at least regarding their effect on the dredge-up efficiency. The black line in Fig. 5 shows the combined CE-PDCZ-D models, which clearly represent the sum of the two individual mechanisms. At the lower values of the CBM parameter, the trend follows that of the PDCZ-D models, as there is no significant influence from the CE boundary, while there is the almost step-like increase in the CE-PDCZ-D models at the $f_{\rm CBM} = 0.016$ model, to move away from the PDCZ-D set of models before continuing with the linear increase in λ as the PDCZ-D boundary again entirely dominates the outcome.

5 CONSTRAINING ADDITIONAL MIXING ON THE TP-AGB

The aim of this section is to constrain the extent of additional mixing beyond the formal convective boundaries on the TP-AGB, through the use of observations and the findings of the previous section. This is primarily done through the use of carbon star number counts, the semi-empirical IFMR, and the observed abundances of PG 1159 stars. It is worth emphasizing that all sequences discussed in the following sections include CBM in convective cores during the pre-AGB phase ($f_{\rm CHB} = f_{\rm CHeB} = 0.0174$).

5.1 PG 1159 stars and intershell abundances

The class of post-AGB stars, known as PG 1159 stars, represent the best method of constraining the chemical composition of the intershell region at the end of the TP-AGB lifetime of a star. The observed oxygen abundances, in particular, cannot be explained without the inclusion of some form of additional mixing at the base of the PDCZ, making this particular observable a good place to start in trying to constrain CBM in TP-AGB stars (Herwig et al. 1997; Herwig 2000).

The data shown in Fig. 6 come from the most updated set of surface parameters $\log g$, $\log T_{\rm eff}$ and He, C, and O abundance determinations for PG 1159 stars (Werner, private communication). Masses are derived from the comparison of $\log g$ and $\log T_{\rm eff}$ for each object with theoretical tracks computed by Miller Bertolami & Althaus (2006).

The final intershell abundances of sets of models with varying $f_{\rm PDCZ}$ at the base of the PDCZ are shown in Fig. 6 as a function of final mass, along with a set of models taken from the calculations of the previous section at $Z = 0.02$ (denoted Z02); all other models are for $Z = 0.008$. For each of the $Z = 0.008$ models, the four

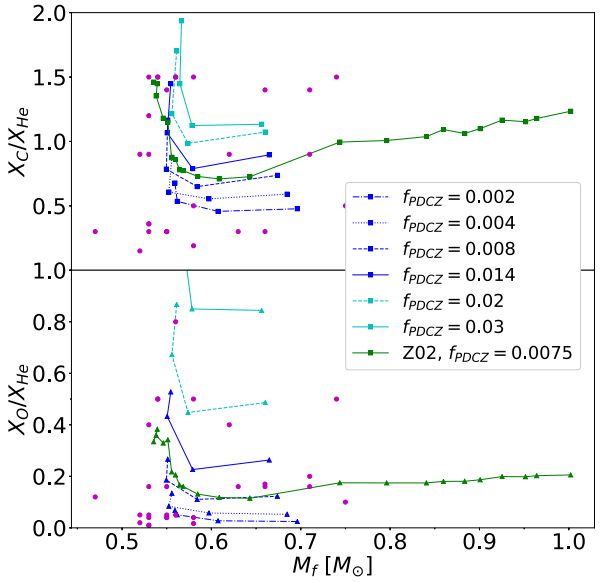

Figure 6. Intershell abundances at the end of the TP-AGB given as the ratio of mass fractions; C/He in the top panel and O/He in the lower panel, as a function of final mass for sets of evolutionary models with the labelled mixing parameter at the base of the PDCZ. 'Z02' indicates models with an initial metal fraction of $Z = 0.02$ while all others are calculated for $Z = 0.008$. Purple circular markers represent observed abundances of PG 1159 stars and were provided by Werner (private communication).

initial masses are 1.6, 2.0, 2.4, and 2.8 $M_\odot$, where the 1.6 $M_\odot$ model always has the highest O/He and C/He values and the 2.8 $M_\odot$ model always has the highest final mass; lines are connecting models in the order of initial mass. As shown in Fig. 6, increasing f_{PDCZ} leads to an increase in the C and also O abundances in the intershell. In agreement with Fig. 4, models with $f_{PDCZ} \leq 0.004$ do not change intershell abundances significantly. Fig. 6 shows that grids of stellar evolution models with different degrees of CBM at the PDCZ are able to reproduce the observed values in PG1159 photospheres.

The models calculated at $Z = 0.02$ with $f_{PDCZ} = 0.0075$ closely match the $Z = 0.008$, $f_{PDCZ} = 0.008$ models. Therefore, having very similar CBM but different metallicity does not seem to impact too much on the predicted intershell abundances. The $Z = 0.02$ models show that the almost constant O/He value against mass continues for all higher mass models calculated. This is both reassuring in terms of a comparable behaviour, which has been seen previously (Miller Bertolami 2016), and that the choice of initial metallicity for the models does not seem to impact too much on the result of the intershell abundances.

The carbon abundances are perhaps less in favour of any particular set of models; however, none of the sequences calculated could produce anything like the spread of values observed there. This may be more generally attributed to the sensitivity of the carbon abundance, which is far more easily mixed into the intershell region.

In conclusion, for the models calculated here, a value of f_{PDCZ} in the range 0.004–0.014 appears to be a limit of possible CBM (in agreement with values suggested in Herwig 2005), with $f_{PDCZ} \sim 0.008$ being able to explain the typical observed carbon and oxygen abundances in PG 1159 stars. However, as the intrinsic spread of PG 1159 carbon and oxygen abundances are larger than errors in mass and abundance determinations, it seems that some object-specific form of mixing (such as rotation-induced mixing) might also be responsible for the observed abundances.

Table 2. Turn-off mass (M_{TO}) along with the number of M-stars (N_M) and C-stars (N_C) taken from table 2 in Girardi & Marigo (2007) for binned LMC cluster data. The minimum and maximum values taken for a given observation of N objects were calculated as discussed in the text.

M_{TO}	N_M	N_M^{min}	N_M^{max}	N_C	N_C^{min}	N_c^{max}
1.66	9	5	12	10	6	13
2.17	22	16	27	32	25	38
2.66	4	1	6	4	1	6

5.2 Carbon star number counts

Rather than using the M- and C-star lifetimes as derived in Girardi & Marigo (2007), it was decided first to compare results directly to the number counts of carbon- and oxygen-rich stars which had been gathered for the purposes of calculating the lifetimes. This is done in order to try and remove some of the assumptions which go into the derivation of the lifetimes, for instance, relying on stellar isochrones having correct ages for all phases of stellar evolution. Of course, errors due to the stellar isochrones still enter into determinations of the initial masses of the objects in a cluster.

The clusters in the sample of Girardi & Marigo (2007) were binned according to the turn-off mass of the cluster for the LMC and SMC separately. Although this represents an excellent sample in terms of AGB stars, the numbers are still very small and so the focus presented here is on three of the data bins taken from their table 2 and which are summarized in Table 2. These points are representative of clusters in the LMC, which have the highest numbers of both M- and C-stars, and also represent the mass range where carbon stars are expected from the stellar evolution models at this metallicity.

The number counts allow for direct comparison with the stellar evolution models, as it is simple to take the time spent as either oxygen-rich or carbon-rich for any given evolutionary track. There is the additional minimum luminosity cut-off of $L_{cut\text{-}off} = 3.336\ L_\odot$, corresponding to $M_{bol} = -3.6$ which was used as an observational limit for ensuring the stars observed were AGB stars above the tip of the RGB. Thus, the fraction of the total number of observed stars which are carbon-rich can be compared to the stellar models. Additionally, to give some indication of how much weight each point should carry, simple upper and lower limits are included in all figures. These limits are taken from considering a Poisson distribution for each number count and taking the maximum and minimum expected number count which would correspond to covering 68 per cent of the distribution. For a given data point, there is both an M-star and C-star number count, so if the minimum M-star count possible (within this very wide tolerance) and maximum C-star count are taken, this should give the maximum observed C-star fraction possible within these limitations, i.e. the maximum C-star fraction is given by

$$\left(\frac{N_C}{N_{Tot}}\right)^{max} = \frac{N_C^{max}}{N_C^{max} + N_M^{min}}. \quad (7)$$

Equally, the minimum C-star fraction can be obtained by taking the maximum value N_M^{max} and the minimum value N_C^{min}. The minimum and maximum values for the number counts taken were as listed in Table 2. It must be stressed that this should not be interpreted as a claim of statistical significance, and was done in the interests of indicating the respective importance of each data point.

Models where CBM only at the base of the PDCZ is active are shown in Fig. 7 in terms of their carbon star fraction. The range of f_{PDCZ} covers 0.002–0.03, and the first point to note is that the

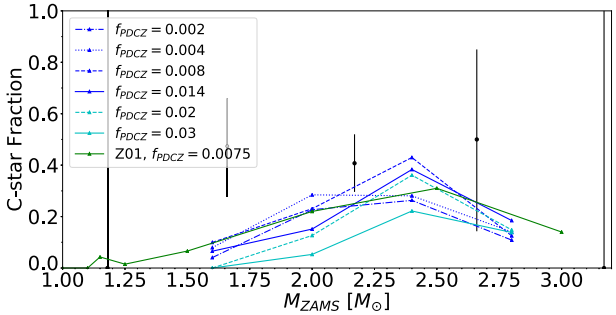

Figure 7. Carbon star fractions for models where CBM is applied only at the base of the PDCZ during the TP-AGB phase, all calculated at $Z = 0.008$, with data points from Table 2. The $Z = 0.01$, $f_{\rm PDCZ} = 0.0075$ models are taken from Miller Bertolami (2016). C-star fractions for the Large Magellanic Cloud are taken from Girardi & Marigo (2007) as discussed in the text.

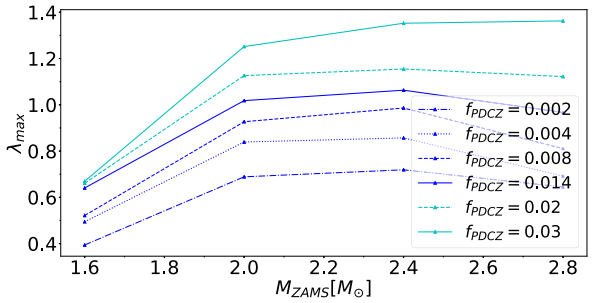

Figure 8. Maximum value for the TDU efficiency parameter, λ, experienced by each model sequence under the assumption of different values of $f_{\rm PDCZ}$.

C-star fraction does not continue to increase with increasing $f_{\rm PDCZ}$ as may have been expected from the results in Section 4.3. Models with $f_{\rm PDCZ}$ in the range 0.004 and 0.02 lead to the largest C-star fractions in Fig. 7, no model appears to satisfactorily reproduce the C-star fractions, even accounting for binning and the coarse grid of models calculated. On the whole, the impression is that additional mixing at the base of the PDCZ alone is not sufficient to reproduce the observed numbers of carbon stars, for any value of $f_{\rm PDCZ}$. Still, as we will see in Section 5.3 a larger C-star fraction can be easily reproduced by a decrease in the C-rich wind prescription adopted in the models.

However, it was seen in the single thermal pulse investigated in Section 4.3 that increasing the mixing parameter at the base of the PDCZ would lead to a strong, almost linear increase in the dredge-up efficiency. Fig. 8 shows the maximum dredge-up efficiency parameter, $\lambda_{\rm max}$, as a function of initial mass for the models where only the base of the PDCZ is active, the behaviour clearly does follow that expected from the single thermal pulse investigation in Section 4.3. Although higher values for $f_{\rm PDCZ}$ do indeed lead to more efficient dredge-up, stronger mixing at the base of the PDCZ also changes the composition of the intershell (Fig. 6), something which is primarily determined during the early thermal pulses as the intershell forms, only changing slightly thereafter. For example, for the 2.4 $M_\odot$, a value of $f_{\rm PDCZ} = 0.03$ leads to a C-to-O ratio of C/O = 1.36, compared to a value of C/O = 3.51 for $f_{\rm PDCZ} = 0.008$. Consequently, the material dredged up to the surface has a higher O content in the case of a large value of $f_{\rm PDCZ}$ delaying the increase of the C/O ratio and the transition to a C-star, thus reducing the C-star fraction predicted by the models (see Fig. 7). Another consequence of the higher O content of the intershell material when

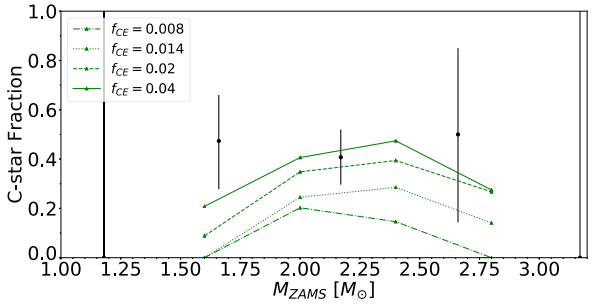

Figure 9. Carbon star fractions for models where CBM is applied only at the base of the CE, all calculated at $Z = 0.008$, with data points from table 2 of Girardi & Marigo (2007) and error bars as discussed in the text.

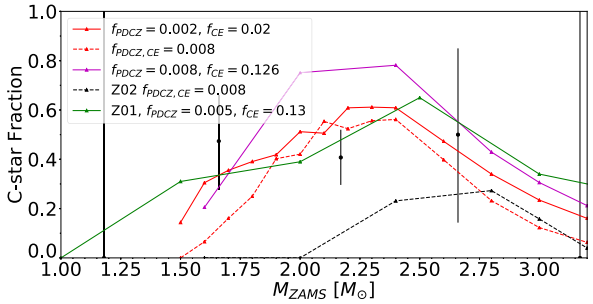

Figure 10. Carbon star fractions for models where CBM is applied at both the base of the PDCZ and the CE, all calculated at $Z = 0.008$ except for the black dashed line at $Z = 0.02$, with data points from table 2 of Girardi & Marigo (2007) and errors as discussed in the text.

$f_{\rm PDCZ}$ is increased, can be seen in the final surface C/O ratios of the models. While the 2.4 $M_\odot$ with $f_{\rm PDCZ} = 0.03$ ends the TP-AGB evolution with a surface value of C/O = 1.3, the 2.4 $M_\odot$ with $f_{\rm PDCZ} = 0.008$ ends the TP-AGB with a much higher surface C/O ratio of C = 3.7.

Fig. 9 shows a similar set of models as Fig. 7, this time displaying the C-star fractions for models with varying $f_{\rm CE}$ between 0.008 and 0.4 at the base of the CE. In this instance, there is a far more straightforward interpretation, with an increase in $f_{\rm CE}$ producing an increased C-star fraction, in almost all cases. Furthermore, there is more readily acceptable agreement with the observed C-star fractions than was the case for the models including only $f_{\rm PDCZ}$. The data point at the lowest mass is perhaps still too high, though it is not unreasonable to think the models are sufficiently close when binning and a better-resolved grid of models are taken into account. Models were also produced for a range of combinations of $f_{\rm PDCZ}$ and $f_{\rm CE}$ in conjunction, with a focus on models where the two are equal. Additionally, models where the value of $f_{\rm CE}$ is higher than $f_{\rm PDCZ}$ were produced following the results from Section 3 where a large discrepancy in the allowed momentum-based CBM at the respective boundaries was suggested. Finally, the preferred value for mixing at the CE, which is derived for the production of the ^{13}C (Herwig et al. 2003), was also considered, namely $f_{\rm CE} = 0.126$, which is higher than would have otherwise been applied. This is sometimes taken alongside a value of $f_{\rm PDCZ} = 0.008$ (Pignatari et al. 2016; Ritter et al. 2018) for the reproduction PG 1159 star abundances. A selection of these models, considered to be of interest, are presented in Fig. 10. The first set of models (magenta line) are those with $f_{\rm PDCZ} = 0.008$, $f_{\rm CE} = 0.126$ and which produce C-star fractions close to 80 per cent at both 2.0 and 2.4 $M_\odot$. Even with the possible influence of binning

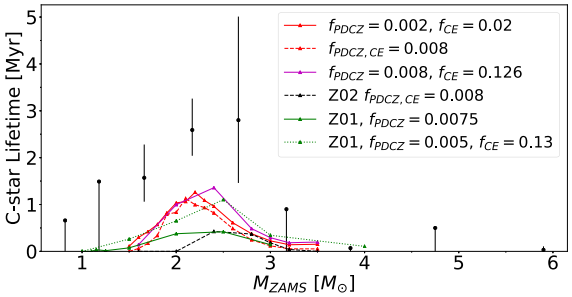

Figure 11. Carbon star lifetimes for the same models as in Fig. 10. In addition, an additional case, computed with LPCODE, and parameters $Z = 0.01$, $f_{\rm PDCZ} = 0.005$ is shown (solid green line). Data points are derived from Girardi & Marigo (2007).

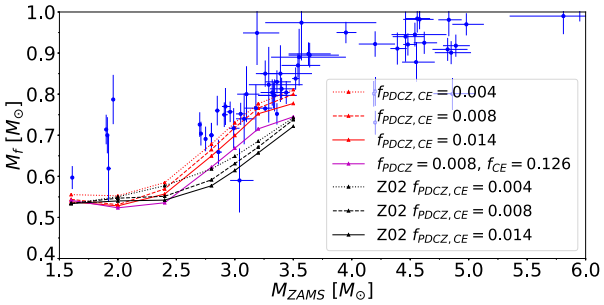

Figure 12. IFMR for models where CBM has been applied at both boundaries for several values, black lines are all calculated at $Z = 0.02$, all others at $Z = 0.008$. Data points are from the semi-empirical IFMR of Cummings et al. (2018).

of the observed data points, and the fact that these two masses do not represent the peak C-star fraction (as exhibited by the other models), this seems to give a first indication that the values sometimes taken for CBM on the TP-AGB (Pignatari et al. 2016; Ritter et al. 2018) do not necessarily agree with evolutionary observational evidence, even if they are well motivated by other means. The black line corresponds to models with $Z = 0.02$, and a choice of $f_{\rm PDCZ} = f_{\rm CE} = 0.008$ to show the influence of metallicity, when compared with the other models with the same choice of $f_{\rm PDCZ}$ and $f_{\rm CE}$. Not only are the C-star fractions significantly lower; in this case, the peak also shifts to higher initial masses, emphasizing that composition plays a significant role in how the models relate to the observations. The other lines correspond to sets of models with $(f_{\rm PDCZ}, f_{\rm CE}) = (0.008, 0.008)$ and $(f_{\rm PDCZ}, f_{\rm CE}) = (0.002, 0.02)$, as well as the LPCODE model with $(f_{\rm PDCZ}, f_{\rm CE}) = (0.005, 0.13)$ which are indeed able to reproduce the observed carbon star fractions. Yet a major inconvenience arises when absolute lifetimes of M-stars and C-stars are considered, as shown in Fig. 11.

As an additional comparison, the C-star lifetimes of the same sets of models as in Fig. 10 are shown again in Fig. 11, in order to directly compare with the data markers derived from the stellar number counts in Girardi & Marigo (2007). Although all the models calculated at $Z = 0.008$ reproduce the basic shape of the observations, the lifetimes are 2–3 times lower than the derived lifetimes, even in the case with $(f_{\rm PDCZ}, f_{\rm CE}) = (0.008, 0.126)$. A similar result was found in LPCODE models by Miller Bertolami (2016). Again, the set of models calculated for $Z = 0.02$ demonstrate how important the initial composition can be in such comparisons. In fact, none of the models calculated here comes close to reproducing the C-star lifetimes. Previously, models calculated with GARSTEC (Kitsikis 2008; Weiss & Ferguson 2009) were in better agreement with these observables. This was in fact due to the individual models calculated at 2 $M_\odot$ experiencing the anomalous phenomenon reported in Wagstaff & Weiss (2018), which increases the C-star lifetime around an initial mass of 2 $M_\odot$ in the models of Wagstaff & Weiss (2018). Additionally, the discrepancy between observationally inferred C- and M-star lifetimes by Girardi & Marigo (2007) and those produced by stellar evolution models might also be related to the AGB boosting effect described by Girardi et al. (2013) for clusters around 1.6 Gyr. As it will be discussed in Section 5.3, this effect might be affecting the derived lifetimes in the 1.66 and 2.17 $M_\odot$ LMC bins of Girardi & Marigo (2007) (Fig. 11) by up to a factor of 2 (Marigo & Girardi, private communication). Thus, significantly reducing the discrepancy with the models.

5.2.1 IFMR

The method of using white dwarfs in open clusters to construct a semi-empirical IFMR is a very useful tool for constraining the TP-AGB evolution. Examples of this method are Salaris et al. (2009), Kalirai, Marigo & Tremblay (2014), and Cummings et al. (2018). In addition, El-Badry et al. (2018) suggested a new method using GAIA data which might help to constrain the low-mass limit of the IFMR.

The IFMR is shown in Fig. 12, where the red lines are models where $f_{\rm PDCZ} = f_{\rm CE}$ for different values at $Z = 0.008$, while the black lines are their counterparts calculated at $Z = 0.02$. The models with $f_{\rm PDCZ} = 0.008$, $f_{\rm CE} = 0.126$ calculated at $Z = 0.008$ are also included. The models with $f_{\rm PDCZ} = f_{\rm CE}$ at $Z = 0.008$ all appear to be in relatively good agreement with the main clump of observed objects around 3 $M_\odot$ and, interestingly, the change arising from the different CBM treatments is significantly less than that arising from the change in initial composition. The models calculated at $Z = 0.02$ were intended to be the 'solar' case for the calculations performed, and hence would allow for reasonable comparison with the IFMR. Although this is likely to be too high a metallicity for solar, it should still be the closest of the models calculated and it would have to be said that none of these models give particularly good agreement with the 3 $M_\odot$ observations.

Additionally, at the lower mass end ($\lesssim$2 $M_\odot$) the models are also at the lower boundary of agreement with the final masses observed. That all sets of models calculated here roughly agree on the final mass of the stars at the lower mass end, and not with observations, suggest something else may be the problem, with mass-loss being the most obvious candidate. However, as seen in the previous section, CBM in the pre-AGB phase can affect the mass of the HFC at the moment of the first thermal pulse and, in that way alter the final mass of the white dwarf.

The models calculated for $(f_{\rm PDCZ}, f_{\rm CE}) = (0.008, 0.126)$ are again shown for comparison. They also appear to be in tension with the observations, even though these models are calculated at $Z = 0.008$. The discrepancy would only get worse if these were also calculated at a higher metallicity of $Z = 0.02$.

For interest, the models from Section 4.1 studying the influence of CBM during phases prior to the TP-AGB are shown in Fig. 13. As these models were all calculated with $Z = 0.02$, it is not surprising that they are below the observational markers in the 3 $M_\odot$ region. The inclusion of core CBM does increase the final masses of the stars, and possibly lead to a functional form which better represents the data, but the final masses still appear to be too low, even though

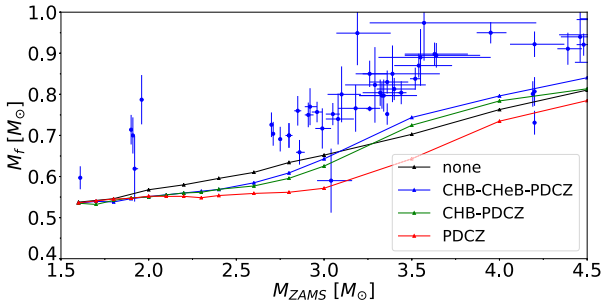

Figure 13. IFMR for models where CBM has been applied during different convective core stages and at the base of the PDCZ for all except the black line. All are calculated at $Z = 0.02$. Data points are as in Fig. 12.

for these models $f_{\rm CE} = 0$ and $f_{\rm PDCZ} = 0.0075$ (apart from the model with no additional mixing). We can conclude that while CBM in pre-AGB stages is in agreement with the IFMR, CBM during the AGB (and in particular at the PDCZ) is clearly disfavoured by the IFMR.

5.3 Tension between different observational constraints

From the comparison of our model intershell abundances and the observed O-abundances of PG1159 stars it is clear that CBM at the PDCZ with a value of $0.004 \lesssim f_{\rm PDCZ} \lesssim 0.014$ is to be preferred (see Fig. 6). This is in agreement with previous findings by Miller Bertolami (2016), Pignatari et al. (2016), and Ritter et al. (2018). However, when the TP-AGB C-star fraction derived from the LMC is considered (Girardi & Marigo 2007), the inclusion of CBM only at the PDCZ gives C-star fractions, which are systematically too low in the range $1.50\,{\rm M}_\odot \lesssim M_{\rm i} \lesssim 2.50\,{\rm M}_\odot$ (see Fig. 7). The agreement with the carbon star fraction is much improved when CBM is included also at the CE (Fig. 9). The agreement is particular good for the sets with $(f_{\rm PDCZ}, f_{\rm CE}) = (0.002, 0.02)$ in case of the GARSTEC code and $(f_{\rm PDCZ}, f_{\rm CE}) = (0.005, 0.13)$ for the LPCODE. The need for CBM at the bottom of the CE is in agreement with the requirements from s-process nucleosynthesis, which suggests values of the order of $f_{\rm CE} = 0.1$–0.2 during TDU episodes (Cristallo et al. 2009; Ritter et al. 2018).

This emerging picture of moderate CBM at the bottom of the PDCZ and a larger value at the bottom of the CE is in agreement with our previous estimation of the possibility of turbulent entrainment at both convective boundaries during thermal pulses (Section 3.2). However, despite this nice agreement, this picture fails miserably to reproduce other observables, such as the total lifetimes of TP-AGB M-stars and the shape of the IFMR.

In fact, when convection is included both at the CE and at the PDCZ, the final masses predicted by stellar evolution sequences fall well below the range indicated by semi-empirical IFMR (Cummings et al. 2018; El-Badry et al. 2018). This suggests that either the TP-AGB is too short or that TDU is too strong, inhibiting the growth of the HFC during the TP-AGB. A similar result was obtained by Kalirai et al. (2014) who found, by calibrating TDU efficiency in TP-AGB envelope models, TDU to be too strong in full stellar evolution models. This conclusion is in agreement with the indications coming from the absolute lifetimes of C- and M-stars predicted by these model sequences (see Figs 11 and 14, and also Miller Bertolami 2016).

Fig. 14 highlights these tensions between different observables in the case of a $M_{\rm i} = 2.2\,{\rm M}_\odot$ sequence (which is the most unfavourable

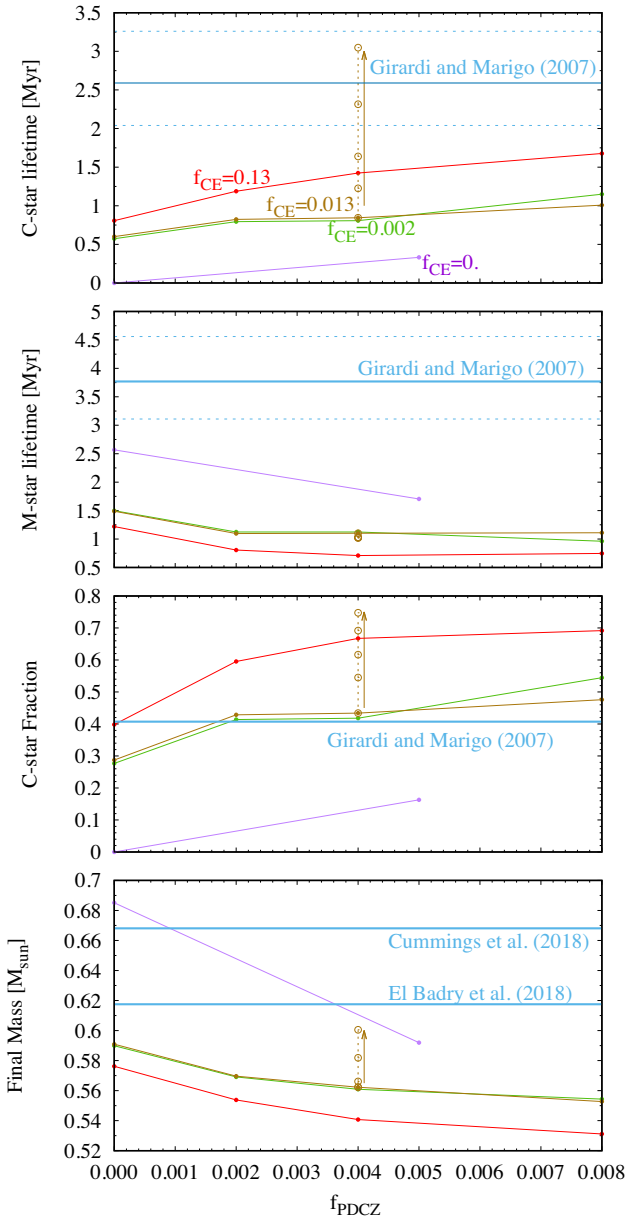

Figure 14. Dependence of different properties of TP-AGB stellar evolution models with $M_{\rm i} = 2.2$ M$_\odot$ on the values of the CBM intensity at the pulse-driven convection zone ($f_{\rm PDCZ}$) and convective envelope ($f_{\rm CE}$) as compared with observationally derived values from clusters in the Large Magellanic Cloud (Girardi & Marigo 2007) and the semi-empirical IFMR of galactic open clusters (Cummings et al. 2018; El-Badry et al. 2018). Open symbols correspond to the sequences ($f_{\rm CE} = 0.013$ and $f_{\rm PDCZ} = 0.004$) computed with a reduction of the mass-loss rate by a factor 2, 4, 8, and 16 shown in Fig. 15. The arrows indicate the how values change as mass-loss rates are decreased.

case). In order to reproduce the expected final masses from semi-empirical IFMR and TP-AGB lifetimes (in particular M-stars) models would need to have no CBM at neither the PDCZ nor the CE.[4] On the contrary, in order to reproduce the C-star fraction, PG1159 abundances,and s-process nucleosynthesis, CBM is needed at both convective boundaries. This is in line with the conclusions

[4]Also, O-rich winds on the TP-AGB would need to be reduced.

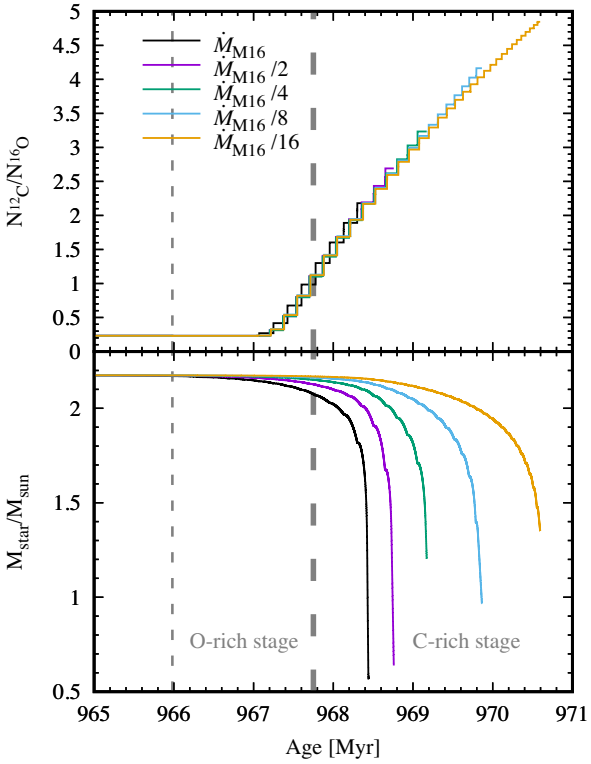

Figure 15. Evolution of the $M_{\rm ZAMS} = 2.2\,{\rm M}_{\odot}$ model ($f_{\rm CE} = 0.013$ and $f_{\rm PDCZ} = 0.004$, see Fig. 14) during the TP-AGB under the assumption of different mass-loss intensities. Black, purple, green, blue, and orange lines correspond to sequences computed with $\dot{M} = \dot{M}_{\rm M16}$, $\dot{M}_{\rm M16}/2$, $\dot{M}_{\rm M16}/4$, $\dot{M}_{\rm M16}/8$, and $\dot{M}_{\rm M16}/16$ where $\dot{M}_{\rm M16}$ corresponds to the TP-AGB wind recipes adopted by Miller Bertolami (2016). The upper panel shows evolution of the C/O ratio against time, while the lower panel shows that of the stellar mass. Vertical thin and thick dashed lines indicate the beginning of the TP-AGB, and the point at which the models transform from an O-rich to a C-rich surface composition, respectively.

from the recent study by Pastorelli (2018), Pastorelli et al. (2019) on the basis of evolutionary TP-AGB envelope models.

It is important to note that the well-known uncertainties in the strength of TP-AGB winds do not alter this conclusion, as they do not reduce these tensions. In fact, while the long C-stars lifetimes derived by (Girardi & Marigo 2007) can indeed be accommodated by reducing C-rich winds on the TP-AGB models (see Figs 14 and 15), the situation is very different for the length of the M-star phase of the same sequences. Contrary to what happens in lower mass AGB stars that do not experience 3DUP, or in more massive stars where HBB keeps the surface composition O-rich, the length of the M-star phase of stellar models that form C-rich stars is almost exclusively determined by the intensity of 3DUP. This is because it is 3DUP that dominates the timing at which the surface composition is transformed from an O-dominated atmosphere (C/O $<$ 1) to a C-dominated one (C/O $>$ 1), ending the M-star phase (see Fig. 15). Such transformation depends on the amount of C dredged-up to the surface, and – in light of previous discussions – on the assumptions about CBM at the bottom of the CE and the PDCZ, but not on the intensity of winds. The only role that winds can play in this context is to reduce the H-rich envelope, such that a given mass of carbon dredged-up to the surface leads to a larger enhancement of photospheric C due to a lower dilution. Such an effect would shorten the O-rich TP-AGB phase, instead of lengthening it. In fact, given that standard mass-loss prescriptions imply a rather small erosion of the envelope during the O-rich phase (see Fig. 15) our estimations of the M-star lifetime can be understood as the upper limit for each given assumption of CBM. The fact that mass-loss intensity does not affect the conclusion of the previous paragraphs can be appreciated in Fig. 15, where we show the result of varying the intensities of winds ($\dot{M}_{\star}$) for the sequences discussed in Fig. 14. As can be seen in the lower panel of Fig. 15, our standard mass-loss recipe ($\dot{M}_{\rm M16}$, Miller Bertolami 2016) leads to a reduction of the mass of the star of less than 10 per cent during the O-rich AGB phase. As a consequence, a reduction in the wind prescription only leads to a very slight decrease in the pollution of the surface by dredged-up carbon, and all sequences transform into C-rich objects at the same time ($t \sim 967.8$ Myr, see upper panel in Fig. 15). Clearly, this experiment demonstrates that the tensions arising from the short M-star lifetimes of intermediate-mass stars (second panel from top of Fig. 14) cannot be resolved by invoking lower wind efficiencies. In addition, while longer C-star lifetimes can be reproduced by decreasing the mass-loss rates, due to the immunity of the M-star lifetimes to mass-loss this would lead to a very serious discrepancy in the C-star fraction, as shown in Fig. 14. Needless to say, the use of more intense winds would lead to a faster reduction of the H-rich envelope mass and to a more intense pollution by C, leading to a shortening of the O-rich TP-AGB phase.

However, an alternative explanation for the previous discrepancy might exist, which is related to the so-called AGB boosting effect described by Girardi et al. (2013). Although in principle the AGB boosting effect should affect stellar lifetimes derived for clusters in the very narrow age range between ∼1.57 and ∼1.66 Gyr (corresponding to initial masses in the range between $\sim$ 1.75 and $\sim 1.8\,{\rm M}_{\odot}$) for the LMC, the actual impact in the stellar lifetimes derived by Girardi & Marigo (2007) is broader due to the adopted binning strategy. Specifically, the clusters NGC 1651, NGC 1652, NGC 1751, NGC 1846, NGC 1856, NGC 1978, NGC 2154, NGC 2173, and NGC 2231 in the LMC (as well as clusters NGC 151, NGC 411, and NGC 419 in the SMC) might be affected by AGB boosting, and due to the binning strategy these clusters are included in both the 1.66 and 2.17 ${\rm M}_{\odot}$ bins for the LMC in (see table 2 of Girardi & Marigo 2007). In particular, the LMC lifetimes for 2.17 ${\rm M}_{\odot}$ adopted for the discussion of the present section could be dominated by clusters affected by the AGB boosting effect, strongly reducing the previously discussed discrepancy. Marigo & Girardi (private communication) estimate that lifetimes in these particular bins of (Girardi & Marigo 2007) might be overestimated by up to a factor 2, although a detailed study is required to assess whether this is the case or not.

6 CONCLUDING REMARKS

We have performed an extensive exploration of the impact of CBM on the predictions of stellar evolution models for the TP-AGB phase. In particular, we have not only explored the impact of CBM during the TP-AGB but also the impact of CBM during previous evolutionary stages on the predictions of TP-AGB stellar models. Our study shows that CBM on the pre-AGB phase has a significant impact on the evolution of TP-AGB models, affecting TDU, HBB, and also the IFMR of the models. This result indicates that studies that aim to link AGB or PNe abundances to the initial stellar progenitor masses, or ages of the host population, should rely on stellar models that include CBM at all pre-AGB phases. This is in agreement with recent hints of HBB taking place in stars with

initial masses as low as $M_{\rm ZAMS} \sim 3\,{\rm M}_{\odot}$ (Fang et al. 2018; Henry et al. 2018; Davis et al. 2019)

As part of this study, we have explored a recent argument by Lattanzio et al. (2017) that buoyancy prevents momentum-driven overshoot at the base of the PDCZ, and shown that, while this is true, this argument also suggest that momentum-driven overshoot cannot happen at the bottom of the CE, where it is necessary to form the ^{13}C pocket required for s-process nucleosynthesis. Therefore, we also performed an estimation of the intensity of turbulent entrainment during thermal pulses both at the bottom of the PDCZ and the CE and proved that, contrary to what happens to momentum-driven overshoot, turbulent entrainment seems to be quite capable of producing CBM on the TP-AGB.

We confirm here that oxygen surface abundances in PG1159-type stars can be reproduced with stellar models that include CBM at the PDCZ with values $f_{\rm PDCZ} = 0.004$–0.014, although the large spread in individual PG1159 abundances also suggest the existence of some object-specific mixing, like rotation-induced mixing, might also be required. Our experiments also show that the C-star fraction derived by (Girardi & Marigo 2007) is better reproduced by models that include CBM at the bottom of the CE, and have a lower intensity of C-rich winds than adopted in our standard models (Weiss & Ferguson 2009; Miller Bertolami 2016). Regarding the CBM during the TP-AGB we have found that the combined influence of $f_{\rm PDCZ}$ and $f_{\rm CE}$ on the TDU efficiency behaves as the linear superposition of the individual influences of CBM at both convective borders (Fig. 4).

These results mentioned above show that CBM on the TP-AGB can be calibrated to reproduce some key observables. Unfortunately, a very different picture arises when the absolute duration of the TP-AGB phase is considered. Stellar evolution models that include CBM during the TP-AGB predict systematically short TP-AGB lifetimes. This is mostly due to the development of very efficient TDU episodes that considerably shorten the lifetime of the TP-AGB star as an O-rich object. This is in agreement with the results recently published by Pastorelli et al. (2019).

We have explored many different observables both on the AGB and post-AGB phases and shown that strong tensions arise that make it impossible for the stellar models to simultaneously reproduce all of them. More specifically, stellar evolution models that include CBM in the way of an exponentially decaying diffusion coefficient are unable to simultaneously reproduce the M- and C-star lifetimes and C-star fractions observed in the clusters of the LMC, the O-abundances measured at the surface of PG1159 stars, the size of the ^{13}C pocket as required from s-process nucleosynthesis and the IFMR as determined from semi-empirical methods. One of the key observables in this regard is the length of the TP-AGB phase, as derived from stellar counts in LMC clusters (Girardi & Marigo 2007). It is possible that TP-AGB lifetimes coming from number counts in globular clusters of the LMC are overestimated by up to a factor of two in the case of the $M_{\rm i} = 1.66$ and $2.17\ {\rm M}_{\odot}$ bins due to the cluster binning and the AGB boosting effect (Girardi et al. 2013). If this is the case, most of this tensions would be significantly reduced. On the contrary, if the relatively long TP-AGB lifetimes derived by (Girardi & Marigo 2007) are supported by future studies this would cast doubt on our current ability to produce accurate models for the AGB and post-AGB phases, as well as to produce reliable yields from AGB nucleosynthesis. Alternative CBM recipes need to be developed and tested for the TP-AGB. In particular time-dependent mixing schemes based on the convective entrainment picture of Meakin & Arnett (2007), and the impact of rotationally induced mixing on the TP-AGB are worth exploring.

ACKNOWLEDGEMENTS

We thank the referee for her/his very detailed reports and for pointing to us the possible impact of the AGB boosting effect in our analysis. This work was enhanced due to the Deutscher Akademischer Austausch Dienst (DAAD) and was supported by the DFG-Cluster of Excellence 'Ursprung und Struktur des Universums'. MMMB is partially supported by Agencia Nacional de Promocion Cientifica y Tecnologica through grant PICT-2016-0053 and by the Ministerio de Ciencia y Tecnologia e Innovacion Productiva/Deutscher Akademischer Austauschdienst bilateral co-operation program through grant DA/16/07. MMMB also thanks the visitor program from the Max-Planck-Institut für Astrophysik. This research has made use of NASA's Astrophysics Data System.

REFERENCES

Andrews J. J., Agüeros M. A., Gianninas A., Kilic M., Dhital S., Anderson S. F., 2015, ApJ, 815, 63
Baraffe I., Pratt J., Goffrey T., Constantino T., Folini D., Popov M. V., Walder R., Viallet M., 2017, ApJ, 845, L6
Bossini D. et al., 2015, MNRAS, 453, 2290
Cassisi S., Salaris M., Irwin A. W., 2003, ApJ, 588, 862
Cassisi S., Potekhin A. Y., Pietrinferni A., Catelan M., Salaris M., 2007, ApJ, 661, 1094
Castellani V., Giannone P., Renzini A., 1971, Ap&SS, 10, 340
Castellani V., Chieffi A., Tornambe A., Pulone L., 1985, ApJ, 296, 204
Charpinet S. et al., 2011, A&A, 530, A3
Claret A., 2007, A&A, 475, 1019
Constantino T., Campbell S. W., Christensen-Dalsgaard J., Lattanzio J. C., Stello D., 2015, MNRAS, 452, 123
Constantino T., Campbell S. W., Lattanzio J. C., van Duijneveldt A., 2016, MNRAS, 456, 3866
Constantino T., Campbell S. W., Lattanzio J. C., 2017, MNRAS, 472, 4900
Cristallo S., Straniero O., Gallino R., Piersanti L., Domínguez I., Lederer M. T., 2009, ApJ, 696, 797
Cristallo S., Straniero O., Piersanti L., Gobrecht D., 2015, ApJS, 219, 40
Cummings J. D., Kalirai J. S., Tremblay P.-E., Ramirez-Ruiz E., Choi J., 2018, ApJ, 866, 21
Davis B. D., Bond H. E., Ciardullo R., Jacoby G. H., 2019, ApJ, 884, 115
De Gerónimo F. C., Battich T., Miller Bertolami M. M., Althaus L. G., Córsico A. H., 2019, A&A, 630, A100
Ekström S. et al., 2012, A&A, 537, A146
El-Badry K., Rix H.-W., Weisz D. R., 2018, ApJ, 860, L17
Fang X. et al., 2018, ApJ, 853, 50
Ferguson J. W., Alexander D. R., Allard F., Barman T., Bodnarik J. G., Hauschildt P. H., Heffner-Wong A., Tamanai A., 2005, ApJ, 623, 585
Freytag B., Ludwig H.-G., Steffen M., 1996, A&A, 313, 497
Gabriel M., Noels A., Montalbán J., Miglio A., 2014, A&A, 569, A63
Girardi L., Marigo P., 2007, A&A, 462, 237
Girardi L., Marigo P., Bressan A., Rosenfield P., 2013, ApJ, 777, 142
Grevesse N., Noels A., 1993, in Prantzos N., Vangioni-Flam E., Casse M., eds, Origin and Evolution of the Elements, Cambridge University Press, Cambridge, p. 15
Groenewegen M. A. T., Whitelock P. A., Smith C. H., Kerschbaum F., 1998, MNRAS, 293, 18
Groenewegen M. A. T., Sloan G. C., Soszyński I., Petersen E. A., 2009, A&A, 506, 1277
Haft M., Raffelt G., Weiss A., 1994, ApJ, 425, 222
Henry R. B. C., Stephenson B. G., Miller Bertolami M. M., Kwitter K. B., Balick B., 2018, MNRAS, 473, 241
Herwig F., 2000, A&A, 360, 952
Herwig F., 2005, ARA&A, 43, 435
Herwig F., Bloecker T., Schoenberner D., El Eid M., 1997, A&A, 324, L81
Herwig F., Blöcker T., Langer N., Driebe T., 1999, A&A, 349, L5
Herwig F., Langer N., Lugaro M., 2003, ApJ, 593, 1056

Herwig F., Freytag B., Fuchs T., Hansen J. P., Hueckstaedt R. M., Porter D. H., Timmes F. X., Woodward P. R., 2007, in Kerschbaum F., Charbonnel C., Wing R. F., eds, ASP Conf. Ser. Vol. 378, Why Galaxies Care About AGB Stars: Their Importance as Actors and Probes. Astron. Soc. Pac., San Francisco, p. 43
Higl J., Weiss A., 2017, A&A, 608, A62
Hurlburt N. E., Toomre J., Massaguer J. M., Zahn J.-P., 1994, ApJ, 421, 245
Iglesias C. A., Rogers F. J., 1996, ApJ, 464, 943
Itoh N., Mitake S., Iyetomi H., Ichimaru S., 1983, ApJ, 273, 774
Jones S., Ritter C., Herwig F., Fryer C., Pignatari M., Bertolli M. G., Paxton B., 2016, MNRAS, 455, 3848
Kalirai J. S., Marigo P., Tremblay P.-E., 2014, ApJ, 782, 17
Kamath D., Karakas A. I., Wood P. R., 2012, ApJ, 746, 20
Karakas A. I., 2014, MNRAS, 445, 347
Karakas A. I., Lattanzio J. C., 2007, Publ. Astron. Soc. Aust., 24, 103
Karakas A. I., Lugaro M., 2016, ApJ, 825, 26
Kippenhahn R., Weigert A., Weiss A., 2012, Stellar Structure and Evolution. Springer, Berlin
Kitsikis A., 2008, PhD thesis, Ludwig-Maximilians-Universität München
Lattanzio J. C., Tout C. A., Neumerzhitckii E. V., Karakas A. I., Lesaffre P., 2017, Mem. Soc. Astron. Ital., 88, 248
Lau H. H. B., Gil-Pons P., Doherty C., Lattanzio J., 2012, A&A, 542, A1
Lugaro M., Herwig F., Lattanzio J. C., Gallino R., Straniero O., 2003, ApJ, 586, 1305
Madonna S. et al., 2018, ApJ, 861, L8
Maeder A., Meynet G., 1991, A&AS, 89, 451
Meakin C. A., Arnett D., 2007, ApJ, 667, 448
Miller Bertolami M. M., 2015, in Dufour P., Bergeron P., Fontaine G., eds, ASP Conf. Ser. Vol. 493, 19th European Workshop on White Dwarfs. Astron. Soc. Pac., San Francisco, p. 83
Miller Bertolami M. M., 2016, A&A, 588, A25
Miller Bertolami M. M., Althaus L. G., 2006, A&A, 454, 845
Mocák M., Müller E., Weiss A., Kifonidis K., 2009, A&A, 501, 659
Pastorelli G., 2018, PhD thesis, Department of Physics and Astronomy, University of Padova
Pastorelli G. et al., 2019, MNRAS, 485, 5666
Pignatari M. et al., 2016, ApJS, 225, 24
Pratt J., Baraffe I., Goffrey T., Constantino T., Viallet M., Popov M. V., Walder R., Folini D., 2017, A&A, 604, A125
Reimers D., 1975, Mem. Soc. R. Sci. Liege, 8, 369
Ritter C., Herwig F., Jones S., Pignatari M., Fryer C., Hirschi R., 2018, MNRAS, 480, 538
Rogers F. J., Swenson F. J., Iglesias C. A., 1996, ApJ, 456, 902
Salaris M., Cassisi S., 2017, R. Soc. Open Sci., 4, 170192
Salaris M., Serenelli A., Weiss A., Miller Bertolami M., 2009, ApJ, 692, 1013
Schaller G., Schaerer D., Meynet G., Maeder A., 1992, A&AS, 96, 269
Schröder K. P., Cuntz M., 2005, ApJ, 630, L73
Schroder K.-P., Pols O. R., Eggleton P. P., 1997, MNRAS, 285, 696
Stancliffe R. J., Fossati L., Passy J.-C., Schneider F. R. N., 2015, A&A, 575, A117
Stothers R. B., Chin C.-W., 1992, ApJ, 390, 136
van Loon J. T., Cioni M.-R. L., Zijlstra A. A., Loup C., 2005, A&A, 438, 273
Viallet M., Meakin C., Prat V., Arnett D., 2015, A&A, 580, A61
Wachter A., Schröder K.-P., Winters J. M., Arndt T. U., Sedlmayr E., 2002, A&A, 384, 452
Wagstaff G., Weiss A., 2018, MNRAS, 477, 4824
Weiss A., Ferguson J. W., 2009, A&A, 508, 1343
Weiss A., Schlattl H., 2008, Ap&SS, 316, 99

This paper has been typeset from a TEX/LATEX file prepared by the author.